Since January 2020 Elsevier has created a COVID-19 resource centre with free information in English and Mandarin on the novel coronavirus COVID-19. The COVID-19 resource centre is hosted on Elsevier Connect, the company's public news and information website.

Computational and Theoretical Chemistry 1199 (2021) 113215

Contents lists available at ScienceDirect

Computational and Theoretical Chemistry

journal homepage: www.elsevier.com/locate/comptc

Computational analysis of functional monomers used in molecular imprinting for promising COVID-19 detection

Hasan Cubuk [a], Mehmet Ozbil [b], Pinar Cakir Hatir [a,*]

[a] Istanbul Arel University, Department of Biomedical Engineering, Bioinspired Functional Polymers and Nanomaterials Laboratory, 34537 Buyukcekmece, Istanbul, Turkey
[b] Gebze Technical University, Institute of Biotechnology, 41400 Gebze, Kocaeli, Turkey

ARTICLE INFO

Keywords:
Molecular imprinting
SARS-CoV-2
COVID-19
Computational analyses
Molecular interactions

ABSTRACT

Today, severe acute respiratory syndrome coronavirus 2 (SARS-CoV-2) has recently caused a severe outbreak worldwide. There are still several challenges in COVID-19 diagnoses, such as limited reagents, equipment, and long turnaround times. In this research, we propose to design molecularly imprinted polymers as a novel approach for the rapid and accurate detection of SARS-CoV-2. For this purpose, we investigated molecular interactions between the target spike protein, receptor-binding domain of the virus, and the common functional monomers used in molecular imprinting by a plethora of computational analyses; sequence analysis, molecular docking, and molecular dynamics (MD) simulations. Our results demonstrated that AMPS and IA monomers gave promising results on the SARS-CoV-2 specific TEIYQAGST sequence for further analysis. Therefore, we propose an epitope approach-based synthesis route for specific recognition of SARS-CoV-2 by using AMPS and IA as functional monomers and the peptide fragment of the TEIYQAGST sequence as a template molecule.

1. Introduction

Coronaviruses are a group of enveloped viruses that can infect human hosts and cause respiratory diseases. Among them, severe acute respiratory syndrome coronavirus 2 (SARS-CoV-2) has recently caused a severe outbreak around the world, known as a pandemic of coronavirus disease 2019 (COVID-19), and infected more than 80,295,030 people as of December 26, 2020 [1–3]. It is clear that developing rapid, accurate, and cost-effective diagnostic testing methods is crucial for monitoring and controlling the pandemic. Currently, several laboratory testing methods are applied to diagnose SARS-CoV-2-infected patients; real-time reverse transcriptase-polymerase chain reaction (RT-PCR), enzyme-linked immunoassays (EIA), and serum viral neutralization (SVN) assays [4,5]. However, there are still several challenges in COVID-19 diagnosis. For instance, the limited availability of reagents, equipment and the long turnaround times have encouraged researchers to develop other technologies. Therefore, new methods like isothermal nucleic acid amplification, next generation sequencing, and CRISPR assays are conducted for detection [4,6,7]. The aim of this study is to design molecularly imprinted polymers (MIPs) for the early and accurate detection of SARS-CoV-2-infected patients as a novel approach (Fig. 1).

Molecularly imprinted polymers are tailor-made materials capable of binding specific target molecules selectively [8]. As MIPs have a specific memory for target molecules, they can be used in many applications such as separation [9], biosensor [10], chromatography [11], drug delivery systems [12]. The molecular imprinting theory is based on the complex formation between the functional monomers and the target molecules, followed by the formation of the network in the presence of crosslinkers. Subsequent removal of the target molecules leaves specific recognition sites complementary in shape, size, and chemical functionality to the molecules of interest. Since MIPs are inspired by the molecular recognition mechanism in nature, it is believed that high selectivity and affinity towards the target molecule should be achieved to develop an effective molecular imprinting system [13]. Furthermore, complex steric interactions between the target molecule and the recognition site of the polymer play an essential role in a rigid MIP network. Therefore, strong molecular interactions must be formed between the target molecule and the functional monomers through hydrogen bonding, electrostatic, or hydrophobic interactions. Thus, before polymerization, the interactions between the functional monomers and the template molecule should be investigated to achieve the highest affinity.

In recent years, MIPs are commonly used for detection purposes, in

* Corresponding author.
E-mail address: pinarcakir@arel.edu.tr (P. Cakir Hatir).

https://doi.org/10.1016/j.comptc.2021.113215
Received 31 December 2020; Received in revised form 24 February 2021; Accepted 8 March 2021
Available online 16 March 2021

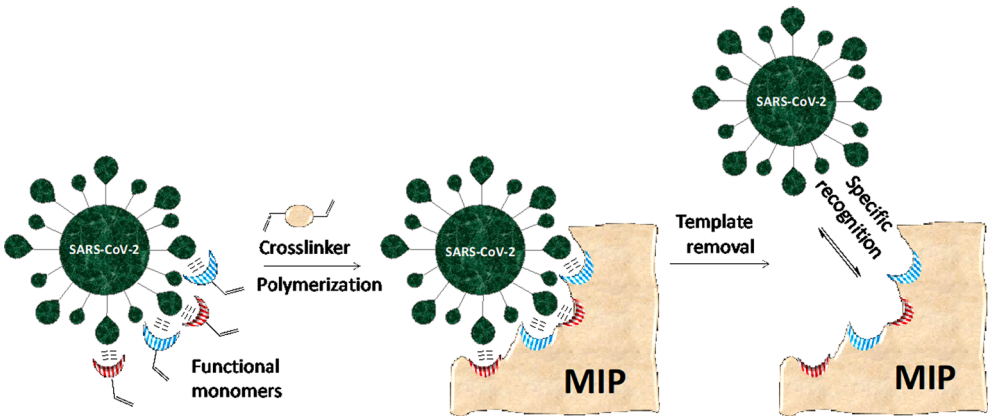

Fig. 1. A schematic representation of molecular imprinting.

particular for viral contamination. Altintas et al. has already reported on the effective use of high affinity molecularly imprinted polymers. They briefly synthesized nanoMIPs targeting *Escherichia coli* bacteriophage (MS2) for the automated capture and analysis of viruses. Their results confirmed the suitability of the nanoMIPs for the detection of viruses [14]. Yang et al. developed a fluorescence molecularly imprinted sensor for Japanese encephalitis virus (JEV) detection [15]. Another fluorescent MIP-based sensor was designed by Luo et al. for simultaneous determination of hepatitis A virus (HAV) and hepatitis B virus (HBV). They demonstrated the potential ability to simultaneously detect multiple viruses in real applications [16]. Zhang et al. developed a magnetic MIP-based optical sensor for specific recognition of trace quantities of hepatitis A virus (HAV) [17]. A QCM based sensor was designed by Jenik et al. using molecular imprinting technique for the human rhinovirus (HRV) and the foot and-mouth disease virus (FMDV) [18]. They indicated that the selectivity and specificity of MIP depends on both geometry and surface chemistry of binding cavities. The selectivity studies, carried out in the presence of different HRV serotypes, showed that MIP has 3–4 times higher affinity towards the template species than other serotypes. The first work regarding MIP-based detection of COVID-19 was recently reported by Raziq et al. [19]. They developed an electrochemical sensor for the recognition of SARS-CoV-2 nucleoprotein using molecular imprinting technique. They demonstrated that the MIP-based sensor was able to detect nucleoprotein which was present in nasopharyngeal swab samples of COVID-19 positive patients. Their promising findings confirm that an efficient, rapid and cost-effective MIP-based diagnostic tool should be developed for the detection of COVID-19.

Proteins are large molecules with complex structures; therefore, it is challenging to create protein imprinted polymers with high selectivity and specificity. Their large size causes diffusion problems in the imprinting process, which can be solved by performing either surface imprinting or imprinting on the nanoscale [20]. Additionally, proteins have chemical and structural complexity and environmental instability. So, protein imprinting should be done in a polar solvent with water-soluble functional monomers. Some polymers may be soluble in a nonpolar solvent; however, their conformations may change due to their structural complexity. The more complex the protein structure, the more critical the monomer selection becomes. It is known that charged monomers can have strong electrostatic interactions with proteins, causing high affinity. Positive and negative charges on the polymer network may form nonspecific interactions for all functional groups carrying the opposite charge on the protein [21]. Despite the possibility of showing nonspecific interactions, charged monomers are frequently preferred for protein imprinting. For instance, 2-acrylamido-2-methyl-propanesulfonic acid (AMPS) was selected as co-monomer for myoglobin-imprinted hydrogels [22], methacrylic acid (MAA) was used for the creation of creatine kinase and ovalbumin-imprinted materials [21], and acrylic acid was employed to produce a variety of target proteins [23]. Experimental results in the literature demonstrated that acrylamide-based monomers accompanied by a small amount of a strongly basic or acidic co-monomer show better protein recognition capacity.

The imprinting strategy is as important as the choice of functional monomer. It is challenging to imprint the entire protein because it is not easy to remove such large molecules from the network's imprinted sites. It is almost impossible to preserve complementary 3D shapes and functional groups. Moreover, due to the size and complexity of its structures, limited diffusion of proteins and slow binding kinetics can occur. A short peptide can be used as a template molecule to overcome these inconveniences known as epitope imprinting [24,25]. Previous studies showed that epitope imprinting has many advantages over traditional protein imprinting, such as facile synthesis of the amino acid sequence, easy removal of amino acid sequence from the polymer

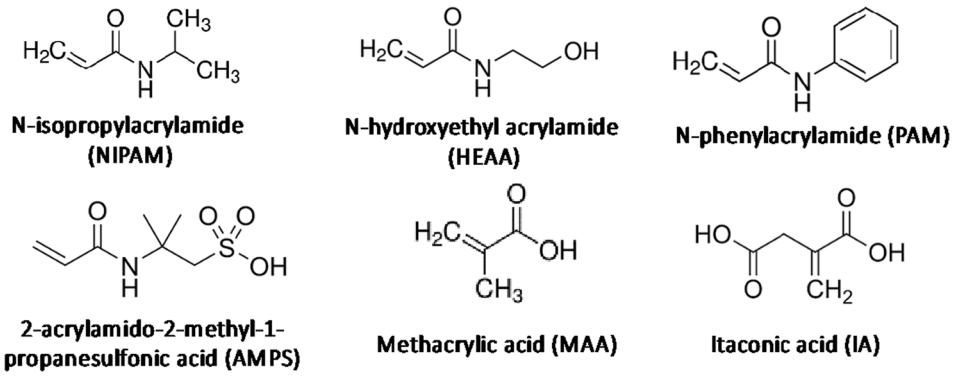

Fig. 2. Functional monomers analyzed in the study.

Table 1
Grid box parameters for molecular docking simulations.

Sequence	Region ID	Grid Box	
		Center (x,y,z)	Size (x,y,z)
SNNLDSKVG (438–446)	1	24, 24, 24	−41, 12, 11
LYRLFRKSNLK (452–462)	2	40, 40, 40	−32, 33, 15
TEIYQAGST (470–478)	3	30, 30, 30	−40, 44, 8
NGVEGF (481–486)	4	24, 24, 24	−46, 44, 10.4
QSYGFQPTNGV (493–503)	5	40, 40, 40	−40, 17, 8

network, and low cost [26]. In this study, an epitope imprinting strategy was adopted instead of assessing the whole protein to evaluate the molecular interactions. For this purpose, only the target spike protein, receptor-binding domain of SARS-CoV-2 virus (SARS-CoV-2 RBD) was selected. It is a long and complicated road to the successful synthesis of MIPs for selective recognition of SARS-CoV-2 virus. Therefore, to cover part of the road, we propose a computational approach to evaluate molecular interactions between the functional monomers and the target molecule to build the strongest interactions and achieve the highest affinity.

The purpose of this research is to investigate molecular interactions between SARS-CoV-2 RBD and the common functional monomers used in molecular imprinting by a plethora of computational analyses; sequence analysis, molecular docking, and molecular dynamics (MD) simulations. This will lead to the construction of a polymer network model to recognize the SARS-CoV-2 virus specifically. *N*-isopropyl acrylamide (NIPAM), *N*-hydroxyethyl acrylamide (HEAA), *N*-phenyl acrylamide (PAM), 2-acrylamido-2-methyl-1-propanesulfonic acid (AMPS), methacrylic acid (MAA), and itaconic acid (IA) were selected as functional monomers with different functional groups (Fig. 2).

2. Methods

2.1. Region selection and molecular docking simulations

The reference sequence of coronavirus spike receptor-binding domain for MERS, SARS-CoV, and SARS-CoV-2 was obtained from the UniProt database. The global alignment was run to detect less conserved regions among three viruses [27–30]. Then, we studied regions having less similarity between the three viruses as a template for MIP studies.

The docking study of the determined monomers over the spike receptor-binding domain complexed with its receptor ACE2 was studied using Autodock-Vina 1.1.2 software [27]. The crystal structure of the coronavirus spike receptor-binding domain complexed with its receptor ACE2 (PDB: 6LZG, 2.5 Å) was downloaded from the Research Collaboratory for Structural Bioinformatics Protein Data Bank (RCSB PDB). Numbering of residues in this crystal structure was followed as residue numbers in this article. Protein receptor structure was prepared for docking using AutoDockTools 1.5.6 software by adding polar hydrogens and Kollman charges [27,31,32]. Grid box parameters for the simulations were provided on Table 1. Docking results were analyzed using BIOVA Discovery Studio Visualizer software [33]. In docking simulations, spike proteins were treated rigid and ligands were flexible.

Small molecules used docking studies were obtained from the PubChem database as in the canonical SMILES format and built on USCF Chimera software. AMPS, MAA, and IA were constructed in their protonated forms, resembling their protonation states at physiological pH value ~ 7.0. Structures of monomers were provided in Fig. 2. Structural minimizations were carried out with Avogadro software to obtain stable conformers. Structural minimizations were directly handled under GAFF forcefield with the steepest descent algorithm [34–36].

2.2. Molecular dynamics (MD) simulations

Following molecular docking simulations, MD simulations were performed to test the stability of monomers AMPS, IA, and PAM. Docking poses located on regions 3 and 4 and provided the highest binding affinities for each monomer were selected as the initial structures. Classical all-atom, free MD simulations were performed using GROMACS 5.0 program, utilizing GROMOS96 54A7 force field [37,38]. Ligand parameters for each ligand were obtained from the PRODRG server for the GROMOS force field [39]. For the RBD domain of SARS-CoV-2, an X-ray diffraction structure with a 2.5 Å resolution (PDB ID: 6LZG) was used [31]. Protein was placed into a cubic box, a box with dimensions of 90.0 Å x 90.0 Å x 90.0 Å. Doing so made sure that all atoms of the protein remained in the box during the simulation. Protonation states of titratable residues were determined by using the PROPKA server at physiological pH value, ~7.0 [40]. The box was filled with explicit single point charge (SPC/E) water molecules [41] and some of them were replaced with Na and Cl ions to neutralize the system. Starting structures were energy-minimized using the steepest descent method. Energy minimized structures were taken to equilibration phases, followed by production phases. MD simulations were carried out with NPT ensemble (constant number of particles (N), pressure (P) and

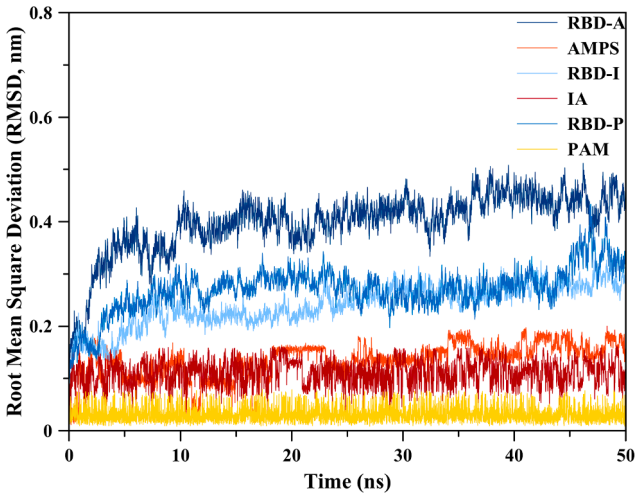

Fig. 3. Root mean square deviation (RMSD) values for AMPS, IA, PAM, and spike protein RBDs. Low values (≤0.4 nm for proteins and ≤ 0.2 nm for monomers) indicated equilibrated proteins and monomers in their binding pockets.

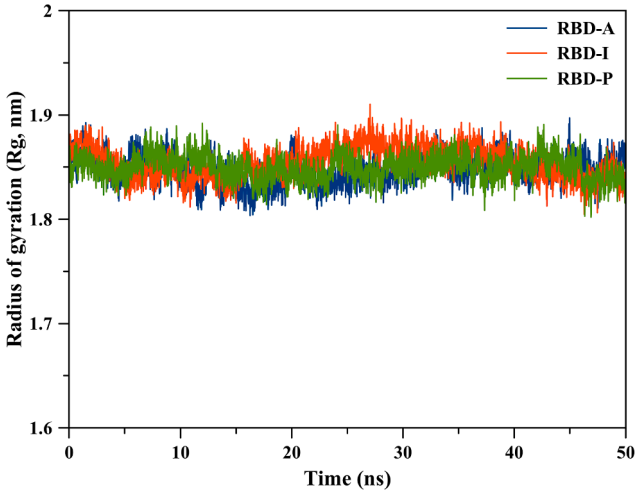

Fig. 4. Radius of gyration values for PAM bound spike protein RBD (RBD-P), IA bound spike protein RBD (RBD-I), and AMPS bound spike protein RBD (RBD-A). Stable graph indicated equilibrated systems and non-significant change in protein compactness.

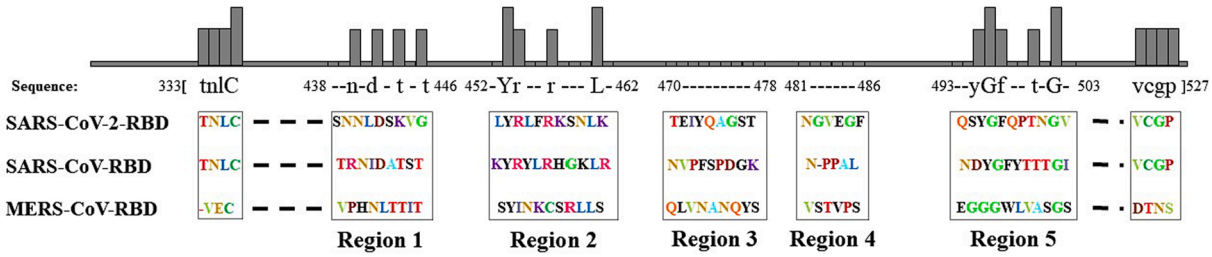

Fig. 5. The rationale for selecting five regions based on sequence dissimilarity.

Table 2
Target region selection criteria.

Region ID	Similarity (1–100%)
1	55.6
2	45.5
3	11.1
4	0.0
5	54.5

temperature (T)). Bond lengths and angles of solvent molecules were constrained by the SETTLE algorithm [42], and bond lengths of amino acid residues were constrained by the LINCS algorithm [43]. Long-range Particle-Mesh Ewald (PME) method was applied to treat electrostatic interactions [44]. The pressure was set to 1 bar with a coupling of 1.0 ps, and water molecules/ions were coupled separately at 300 K. The equation of motion was integrated at 2 fs time steps using the leap-frog algorithm [45]. Production runs were run for 50 ns. The tools available in the GROMACS program package and VMD software were used to analyze the MD trajectories [46]. Root mean square deviation (RMSD) values for spike protein RBDs and AMPS, IA, and PAM were provided in Fig. 3. These low values ($\leq$0.4 nm for proteins and $\leq$ 0.2 nm for monomers) indicated equilibrated proteins and very stable monomers in their binding pockets throughout the simulations. Likewise, for all spike protein RBDs radius of gyration (Rg) values lied between 1.81 nm and 1.91 with very little fluctuation, indicating equilibrated systems (Fig. 4). Moreover, these values showed that there was no significant change in the compactness and folding of proteins upon monomer binding.

3. Results and discussion

To investigate molecular interactions between spike protein, receptor binding domain of SARS-CoV-2 virus (SARS-CoV-2 RBD) and the functional monomers, six monomers (NIPAM, PAM, HEAA, AMPS, MAA, and IA) which are commonly used in protein imprinting were selected [47]. NIPAM, PAM, HEAA, and AMPS are acrylamide-based monomers with uncharged hydrophobic groups of NIPAM and PAM, an uncharged hydrophilic group of HEAA, and acidic functionality of AMPS. In addition to these acrylamide-based monomers, two typical acidic monomers were also chosen to test the acidic group effect on the molecular interactions. MAA consists of one carboxylic acid, and IA consists of two carboxylic acid groups. The selected functional monomers are candidates that can form noncovalent interactions with associated side chains of amino acids such as hydrophobic interactions, aromatic interactions, hydrogen bonding, and electrostatic interactions.

RBDs of three types of coronaviruses were aligned using global alignment algorithms to determine the target regions on SARS CoV-2 RBD, i.e., regions that are specific to SARS-CoV-2 RBD. In this regard, less conserved five regions were defined as a novel targeting region for the molecularly imprinted polymer templates (Fig. 5). Similarities of the regions were calculated as % percent unit based on the local alignment between three types of coronaviruses RBD (Table 2). In this context, SNNLDSKVG, LYRLFRKSNLK, TEIYQAGST, NGVEGF, and QSYGFQPTNGV sequences on SARS-CoV-2 RBD were highlighted as the promising targeting regions. TEIYQAGST and NGVEGF sequences have attracted the attention as they are the least conserved regions among other candidates.

Table 3
Binding affinities and hit scores (in parentheses) from molecular docking simulations of each monomer in different regions. Affinities below cut-off 4.0 kcal/mol were labeled bold.

Binding affinities (kcal/mol)	Region 1 (hit %)	Region 2 (hit %)	Region 3 (hit %)	Region 4 (hit %)	Region 5 (hit %)
AMPS	**−4.4 (90%)**	**−4.6 (20%)**	**−5.4 (30%)**	−3.7 (70%)	**−4.8 (90%)**
IA	**−4.3 (40%)**	**−4.6 (30%)**	**−5.1 (80%)**	−3.5 (50%)	**−4.4 (40%)**
MAA	−3.5 (50%)	−3.5 (10%)	**−4.4 (30%)**	−3.2 (50%)	−3.7 (30%)
NIPAM	−3.4 (30%)	−3.7 (10%)	−3.5 (30%)	−2.9 (60%)	**−4.3 (70%)**
PAM	−3.7 (40%)	**−4.5 (10%)**	**−4.9 (50%)**	**−3.9 (60%)**	**−4.9 (90%)**
HEAA	−3.7 (40%)	−3.9 (30%)	−3.9 (60%)	−3.1 (60%)	**−4.3 (60%)**

Note: Poses interacting only target region were evaluated.

Table 4
Dissociation constants calculated from molecular docking simulations of each monomer in different regions, at 25 °C.

Dissociation constant (K_d)	Region 1	Region 2	Region 3	Region 4	Region 5
AMPS	**5,93E-04**	**4,23E-04**	**1,09E-04**	1,93E-03	**3,02E-04**
IA	**7,02E-04**	**4,23E-04**	**1,82E-04**	2,71E-03	**5,93E-04**
MAA	2,71E-03	2,71E-03	**5,93E-04**	4,50E-03	1,93E-03
NIPAM	3,21E-03	1,93E-03	2,71E-03	7,46E-03	**7,02E-04**
PAM	1,93E-03	**5,01E-04**	**2,55E-04**	**1,38E-03**	**2,55E-04**
HEAA	1,93E-03	**1,38E-03**	**1,38E-03**	**5,32E-03**	**7,02E-04**

Note: Poses interacting only target region were evaluated.

To detect binding affinities of each monomer, we designed docking simulations covering five determined targeting regions (coordinates were given in the methods in detail). Monomers yielded different binding affinities ranging from −2.9 kcal/mol to −5.4 kcal/mol (Table 3). K_i values from these binding affinities were also provided in Table 4. Monomers yielding binding affinity over −4.0 kcal/mol were classified as low-scored and under −4.0 kcal/mole as high-scored monomers. In this regard, AMPS and IA were good candidates for binding to targeting regions except for the NGVEGF sequence (region 4), which is the least similar. Also, PAM was the second suitable binder behind AMPS and IA couple, while other monomers (MAA, NIPAM, and

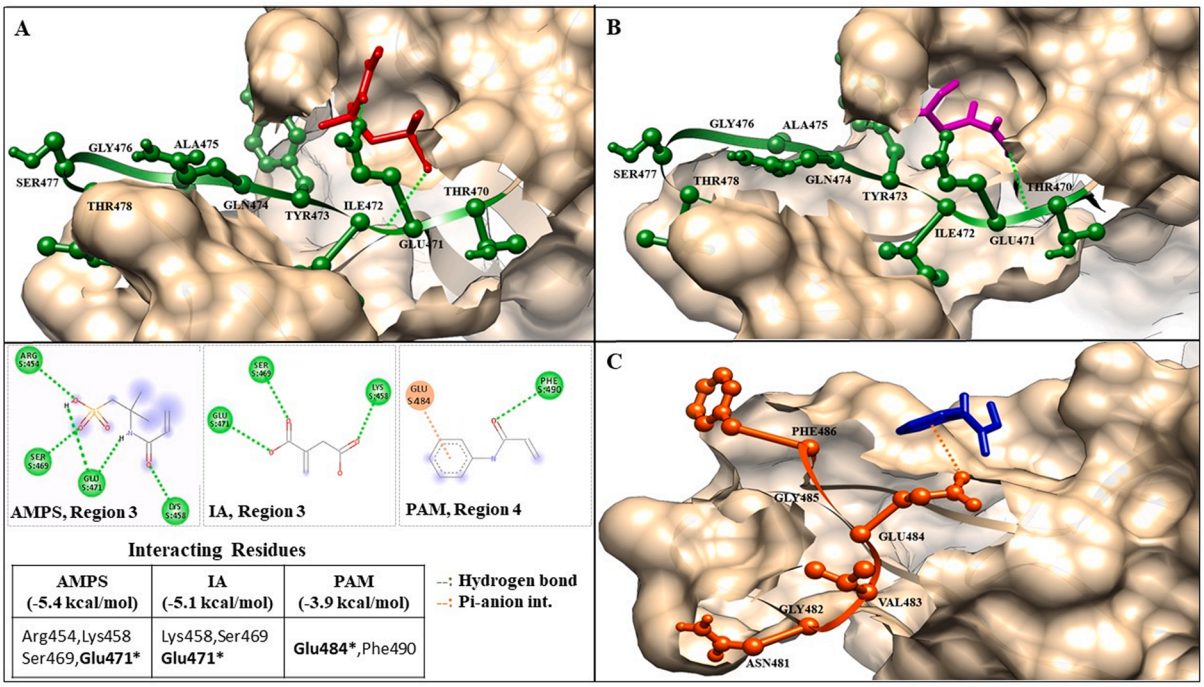

Fig. 6. A) Positions and molecular interactions for AMPS (red) in region 3 (green), B) Positions and molecular interactions for IA (magenta) in region 3, C) Positions and molecular interactions for PAM (blue) in region 4 (orange).

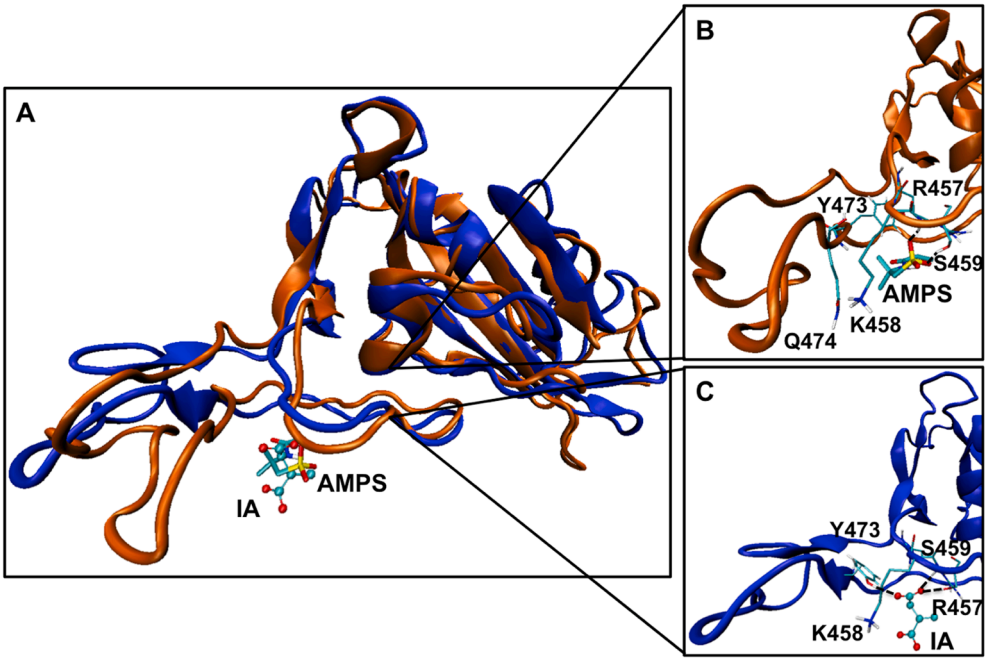

Fig. 7. A) Average structures from 50 ns MD simulations of RBD-AMPS (orange) and RBD-IA (blue) complexes. AMPS was shown with stick, IA with ball and stick representations. B) Zoomed in view of RBD-AMPS interactions. C) zoomed in view of RBD-IA interactions.

HEAA) yielded low binding affinities compared to AMPS, IA, and PAM.

AMPS and IA yielded the highest binding affinities of −5.4 kcal/mol and −5.1 kcal/mol, respectively, on the TEIYQAGST sequence, which is the second less conserved region among others. These binding affinities suggested that AMPS and IA monomers could be better choices to build MIPs on the **TEIYQAGST** sequence. Therefore, AMPS and IA in region 3 have attracted our attention for further analysis. In our analysis, we observed that SARS-CoV-2 RBD residues Arg454, Lys458, Ser469, and Glu471 created hydrogen bonds with AMPS monomer (Fig. 6A). Also, Lys458, Ser469, and Glu471 residues on SARS-CoV-2 RBD interacted with IA through hydrogen bonds were observed (Fig. 6B). Apart from that, we also evaluated region 4 as it has a unique sequence, which is the best targeting region based on the primary analysis. No binding affinity less than −4.0 kcal/mol was reported in this region, but the strongest affinity was achieved with PAM. That's why we also further analyzed this site as an exception in addition to region 3 (Fig. 6C).

AMPS was stable throughout 50 ns MD simulation. It remained interacting with RBD residues Arg457, Lys458, Ser459, Tyr473, and

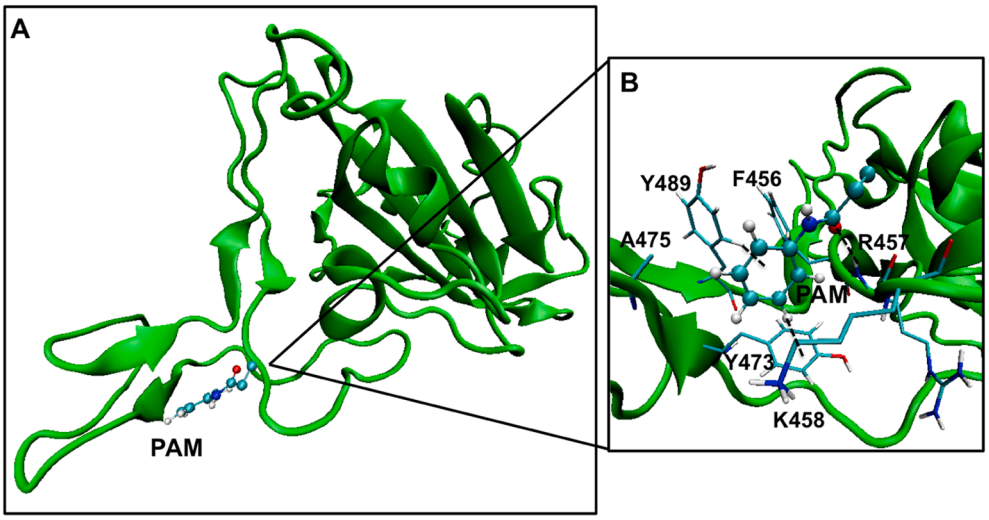

Fig. 8. A) Average structure from 50 ns MD simulations of RBD-PAM. B) Zoomed in view of RBD-PAM interactions.

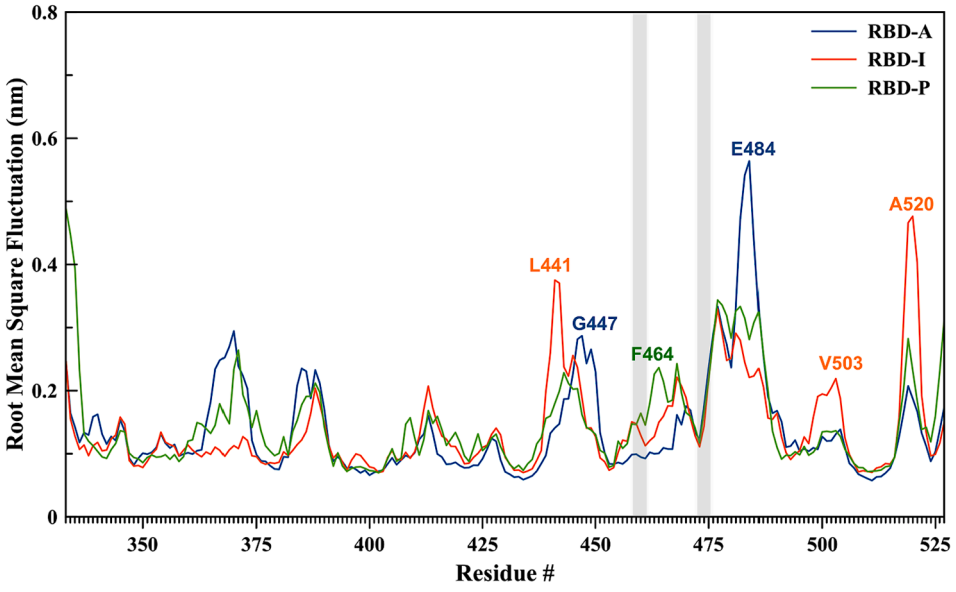

Fig. 9. Root mean square fluctuation (RMSF) values for each RBD residue upon monomer binding throughout the MD simulations. Monomer binding sites, Phe 456-Ser 459 and Tyr 473-Ala 475, were highlighted in gray.

Gln474 (Fig. 7). The sulfonic acid moiety of AMPS made hydrogen bonds with Arg457 and Ser459, whereas the hydrophobic part of the monomer resided in a hydrophobic pocket formed by side carbon chain of Lys 458 and Gln 474, and aromatic phenyl ring of Tyr 473.

Itaconic acid was stable throughout simulations as well. It remained interacting with residues Arg457, Lys458, Ser459, and Tyr473 (Fig. 7). Carboxylic acid moiety made hydrogen bonds with Arg457, Ser459, and Tyr473, while the hydrophobic middle part of the molecule interacted with side-chain carbon atoms of Lys458. MD simulations confirmed that both monomers were stable in their binding pockets, revealed by molecular docking simulations.

N-phenyl acrylamide was not stable in the first few seconds of the MD simulations. Starting from a docking pose in region 4, interacting with residues Glu484, Phe490. However, towards the middle of the simulations, PAM moved to region 3 (Fig. 8). This binding pocket was very similar to the binding pockets for AMPS and IA. Here, the carbonyl group of PAM made hydrogen bond with the side chain of Arg457. Its phenyl ring made CH-π interaction with the aromatic ring of Tyr473 and similarly, Tyr489 made CH-π interaction with its phenyl ring. Moreover, the phenyl ring of PAM lied into the hydrophilic pocket comprised of Phe456, side chain hydrocarbons of Lys458, and Ala475. Root mean square fluctuation (RMSF) values for each spike protein residue were calculated for each monomer-spike protein complex. RMSF provides fluctuation of each residue throughout MD simulations, and it is an indication of the flexibility of that particular residue. RMSF values were provided in Fig. 9, and the common monomer-binding site in RBD was highlighted in gray. These values indicated that the binding of each monomer altered the flexibility of spike protein residues in a similar way except for few residues. AMPS binding increased the flexibility of Gly 447 and Glu 484 residues. IA binding increased the flexibility of Leu 441, Val 503, and Ala 520, whereas PAM binding increased the flexibility of Phe 464. When the flexibility of binding site residues was compared, flexibility of the residues Phe 456-Ser 459 were similar upon IA and PAM binding, but it was reduced slightly upon AMPS binding. On the contrary, the flexibility of the second binding site residues, Tyr 473-Ala 475, was very similar upon binding of all monomers.

We concluded that AMPS and IA are the best functional monomers to design MIPs for SARS-CoV-2 recognition based on the computational

analyses. Not only was region 3 shown to have strong molecular interactions with AMPS and IA, but it was also identified as the second region that was the least conserved of five regions. Our aim is to design a MIP network that will target the SARS-CoV-2 specific peptide target, which has the least similar amino acid sequence in RBDs of three different types of coronaviruses. Also, region 4 was identified as the least conserved region among the five regions. According to docking simulations, the highest affinity was obtained with the monomer PAM provided the highest binding affinity in this region, however, during MD simulations, PAM shifted to region 3. Region 3 contains the amino acid sequence TEIYQAGST, which consists of four uncharged hydrophilic amino acids (T, Y, Q, S), three hydrophobic amino acids (I, A, G), and one acidic amino acid (E). Docking simulations demonstrated that Glu471 formed hydrogen bonds with AMPS and IA, while MD simulations also showed that AMPS created hydrophobic interactions with Gln474 and Tyr473. Based on the docking and MD simulations, we concluded that the molecular interactions with AMPS included Gln474, Tyr473, and Glu471 of the TEIYQAGST sequence.

Consequently, the optimum region for monomer targeting was identified as region 3. The most appropriate functional monomers were determined as AMPS and IA according to the obtained binding affinities. A peptide fragment, including the TEIYQAGST sequence, can be produced as the synthetic epitope template for the sequence recognition approach. One significant benefit of region 3 is that the TEIYQAGST sequence has no complex secondary structure but rather a linear peptide chain (random coil) of nine amino acids. Hence, the peptide chain synthesis with this sequence as an epitope template in laboratory conditions may be straightforward. Finally, we propose an epitope approach-based synthesis route for specific recognition of SARS-CoV-2 by using AMPS and IA as functional monomers and the peptide fragment of the TEIYQAGST sequence as a template molecule.

4. Conclusion

Currently, several laboratory testing methods are applied to diagnose SARS-CoV-2-infected patients. However, there are still several challenges in COVID-19 diagnosis, such as limited availability of reagents, equipment, etc. Therefore, tremendous efforts have been focused on studies for new methods in COVID-19 diagnosis.

For this purpose, we investigated molecular interactions between the target spike protein, receptor-binding domain of SARS-CoV-2 virus, and the common functional monomers used in molecular imprinting by a plethora of computational analyses; sequence analysis, molecular docking, and molecular dynamics (MD) simulations. Our results demonstrated that AMPS and IA monomers, which were actively used in protein imprinting studies gave promising results on the SARS-CoV-2 specific TEIYQAGST sequence for further analysis.

CRediT authorship contribution statement

Hasan Cubuk: Methodology, Software, Data curation, Formal analysis, Writing - original draft. **Mehmet Ozbil:** Conceptualization, Methodology, Software, Data curation, Formal analysis, Writing - original draft. **Pinar Cakir Hatir:** Conceptualization, Methodology, Data curation, Formal analysis, Writing - original draft, Writing - review & editing.

Declaration of Competing Interest

The authors declare that they have no known competing financial interests or personal relationships that could have appeared to influence the work reported in this paper.

Acknowledgments

Authors acknowledge the supercomputing facility TRUBA, hosted by TÜBİTAK ULAKBİM, for computational resources used during MD simulations.

Funding

This research did not receive any specific grant from funding agencies in the public, commercial, or not-for-profit sectors.

Data availability

The raw/processed data required to reproduce these findings cannot be shared at this time due to technical or time limitations.

References

[1] T.S. Fung, D.X. Liu, Human coronavirus: Host-pathogen interaction, Annu. Rev. Microbiol. 73 (2019) 529–557, https://doi.org/10.1146/annurev-micro-020518-115759.
[2] T. Singhal, A Review of Coronavirus Disease-2019 (COVID-19), Indian J. Pediatr. 87 (2020) 281–286, https://doi.org/10.1007/s12098-020-03263-6.
[3] Worldometer, Coronavirus Update (Live): Cases and Deaths from COVID-19 Virus Pandemic, Worldometers. (2020) 1. (accessed October 22, 2020). https://www.worldometers.info/coronavirus/%0Ahttps://www.worldometers.info/coronavirus/?.
[4] R.J. D'Cruz, A.W. Currier, V.B. Sampson, Laboratory Testing Methods for Novel Severe Acute Respiratory Syndrome-Coronavirus-2 (SARS-CoV-2), Front. Cell Dev. Biol. 8 (2020) 468, https://doi.org/10.3389/fcell.2020.00468.
[5] B. Nogrady, How SARS-CoV-2 Tests Work and What's Next in COVID-19 Diagnostics | The Scientist Magazine®, Sci. (2020) Available at: (accessed October 22, 2020). https://www.the-scientist.com/news-o. https://www.the-scientist.com/news-opinion/how-sars-cov-2-tests-work-and-whats-next-in-covid-19-diagnostics-67210.
[6] C.C. Chang, C.C. Chen, S.C. Wei, H.H. Lu, Y.H. Liang, C.W. Lin, Diagnostic devices for isothermal nucleic acid amplification, Sensors (Switzerland) 12 (2012) 8319–8337, https://doi.org/10.3390/s120608319.
[7] J.P. Broughton, X. Deng, G. Yu, C.L. Fasching, V. Servellita, J. Singh, X. Miao, J. A. Streithorst, A. Granados, A. Sotomayor-Gonzalez, K. Zorn, A. Gopez, E. Hsu, W. Gu, S. Miller, C.Y. Pan, H. Guevara, D.A. Wadford, J.S. Chen, C.Y. Chiu, CRISPR–Cas12-based detection of SARS-CoV-2, Nat. Biotechnol. 38 (2020) 870–874, https://doi.org/10.1038/s41587-020-0513-4.
[8] K. Haupt, K. Mosbach, Molecularly imprinted polymers and their use in biomimetic sensors, Chem. Rev. 100 (2000) 2495–2504, https://doi.org/10.1021/cr990099w.
[9] R.I. Boysen, L.J. Schwarz, D.V. Nicolau, M.T.W. Hearn, Molecularly imprinted polymer membranes and thin films for the separation and sensing of biomacromolecules, J. Sep. Sci. 40 (2017) 314–335, https://doi.org/10.1002/jssc.201600849.
[10] V.M. Ekomo, C. Branger, R. Bikanga, A.M. Florea, G. Istamboulie, C. Calas-Blanchard, T. Noguer, A. Sarbu, H. Brisset, Detection of Bisphenol A in aqueous medium by screen printed carbon electrodes incorporating electrochemical molecularly imprinted polymers, Biosens. Bioelectron. 112 (2018) 156–161, https://doi.org/10.1016/j.bios.2018.04.022.
[11] T. Bouvarel, N. Delaunay, V. Pichon, Selective extraction of cocaine from biological samples with a miniaturized monolithic molecularly imprinted polymer and on-line analysis in nano-liquid chromatography, Anal. Chim. Acta 1096 (2020) 89–99, https://doi.org/10.1016/j.aca.2019.10.046.
[12] S.A. Zaidi, Latest trends in molecular imprinted polymer based drug delivery systems, RSC Adv. 6 (2016) 88807–88819, https://doi.org/10.1039/c6ra18911c.
[13] R. Boroznjak, J. Reut, A. Tretjakov, A. Lomaka, A. Öpik, V. Syritski, A computational approach to study functional monomer-protein molecular interactions to optimize protein molecular imprinting, J. Mol. Recognit. 30 (2017), e2635, https://doi.org/10.1002/jmr.2635.
[14] Z. Altintas, M. Gittens, A. Guerreiro, K.A. Thompson, J. Walker, S. Piletsky, I. E. Tothill, Detection of Waterborne Viruses Using High Affinity Molecularly Imprinted Polymers, Anal. Chem. 87 (2015) 6801–6807, https://doi.org/10.1021/acs.analchem.5b00989.
[15] J. Yang, W. Feng, K. Liang, C. Chen, C. Cai, A novel fluorescence molecularly imprinted sensor for Japanese encephalitis virus detection based on metal organic frameworks and passivation-enhanced selectivity, Talanta. 212 (2020), 120744, https://doi.org/10.1016/j.talanta.2020.120744.
[16] L. Luo, F. Zhang, C. Chen, C. Cai, Visual Simultaneous Detection of Hepatitis A and B Viruses Based on a Multifunctional Molecularly Imprinted Fluorescence Sensor, Anal. Chem. 91 (2019) 15748–15756, https://doi.org/10.1021/acs.analchem.9b04001.
[17] F. Zhang, L. Luo, H. Gong, C. Chen, C. Cai, A magnetic molecularly imprinted optical chemical sensor for specific recognition of trace quantities of virus, RSC Adv. 8 (2018) 32262–32268, https://doi.org/10.1039/c8ra06204h.
[18] M. Jenik, R. Schirhagl, C. Schirk, O. Hayden, P. Lieberzeit, D. Blaas, G. Paul, F. L. Dickert, Sensing picornaviruses using molecular imprinting techniques on a quartz crystal microbalance, Anal. Chem. 81 (2009) 5320–5326, https://doi.org/10.1021/ac8019569.
[19] A. Raziq, A. Kidakova, R. Boroznjak, J. Reut, A. Öpik, V. Syritski, Development of a portable MIP-based electrochemical sensor for detection of SARS-CoV-2 antigen,

Biosens. Bioelectron. 178 (2021), 113029, https://doi.org/10.1016/j.bios.2021.113029.
[20] H.R. Culver, N.A. Peppas, Protein-Imprinted Polymers: The Shape of Things to Come? Chem. Mater. 29 (2017) 5753–5761, https://doi.org/10.1021/acs.chemmater.7b01936.
[21] K. Yang, L. Zhang, Z. Liang, Y. Zhang, Protein-imprinted materials: Rational design, application and challenges, Anal. Bioanal. Chem. 403 (2012) 2173–2183, https://doi.org/10.1007/s00216-012-5840-y.
[22] E. Turan, G. Özçetin, T. Caykara, Dependence of protein recognition of temperature-sensitive imprinted hydrogels on preparation temperature, Macromol. Biosci. 9 (2009) 421–428, https://doi.org/10.1002/mabi.200800273.
[23] Y. Saylan, R. Üzek, L. Uzun, A. Denizli, Surface imprinting approach for preparing specific adsorbent for IgG separation, J. Biomater. Sci. Polym. Ed. 25 (2014) 881–894, https://doi.org/10.1080/09205063.2014.911569.
[24] M. Kempe, K. Mosbach, Separation of amino acids, peptides and proteins on molecularly imprinted stationary phases, J. Chromatogr. A. 691 (1995) 317–323, https://doi.org/10.1016/0021-9673(94)00820-Y.
[25] H. Bagán, T. Zhou, N.L. Eriksson, L. Bülow, L. Ye, Synthesis and characterization of epitope-imprinted polymers for purification of human hemoglobin, RSC Adv. 7 (2017) 41705–41712, https://doi.org/10.1039/c7ra07674f.
[26] Y.J. Yan, X.W. He, W.Y. Li, Y.K. Zhang, Nitrogen-doped graphene quantum dots-labeled epitope imprinted polymer with double templates via the metal chelation for specific recognition of cytochrome c, Biosens. Bioelectron. 91 (2017) 253–261, https://doi.org/10.1016/j.bios.2016.12.040.
[27] O. Trott, A.J. Olson, AutoDock Vina: Improving the speed and accuracy of docking with a new scoring function, efficient optimization, and multithreading, J. Comput. Chem. 31 (2009) NA-NA. https://doi.org/10.1002/jcc.21334.
[28] National Institutes of Health - UniProt, S - Spike glycoprotein precursor - Middle East respiratory syndrome-related coronavirus (isolate United Kingdom/H123990006/2012) (MERS-CoV) - S gene & protein, (n.d.). (accessed October 22, 2020). https://www.uniprot.org/uniprot/K9N5Q8.
[29] N.I. of H.- UniProt, S - Spike glycoprotein precursor - Severe acute respiratory syndrome coronavirus 2 (2019-nCoV) - S gene & protein, (n.d.). (accessed October 22, 2020). https://www.uniprot.org/uniprot/P0DTC2.
[30] N.I. of H.- UniProt, S - Spike glycoprotein precursor - Severe acute respiratory syndrome coronavirus (SARS-CoV) - S gene & protein, (n.d.). (accessed October 22, 2020). https://www.uniprot.org/uniprot/P59594.
[31] Q. Wang, Y. Zhang, L. Wu, S. Niu, C. Song, Z. Zhang, G. Lu, C. Qiao, Y. Hu, K. Y. Yuen, Q. Wang, H. Zhou, J. Yan, J. Qi, Structural and Functional Basis of SARS-CoV-2 Entry by Using Human ACE2, Cell 181 (2020) 894–904.e9, https://doi.org/10.1016/j.cell.2020.03.045.
[32] M. Sanner, D. Stoffler, A. Olson, ViPEr, a visual programming environment for Python, Proc. 10th Int. Python Conf. (2002) 103–115.
[33] Dassault Systèmes, BIOVIA Discovery Studio Visualizer, V16.1.0.15350. (2016).
[34] E.F. Pettersen, T.D. Goddard, C.C. Huang, G.S. Couch, D.M. Greenblatt, E.C. Meng, T.E. Ferrin, UCSF Chimera - A visualization system for exploratory research and analysis, J. Comput. Chem. 25 (2004) 1605–1612, https://doi.org/10.1002/jcc.20084.
[35] PubChem, PubChem, (n.d.). (accessed October 22, 2020). https://pubchem.ncbi.nlm.nih.gov/.
[36] M.D. Hanwell, D.E. Curtis, D.C. Lonie, T. Vandermeerschd, E. Zurek, G. R. Hutchison, Avogadro: An advanced semantic chemical editor, visualization, and analysis platform, J. Cheminform. 4 (2012), https://doi.org/10.1186/1758-2946-4-17.
[37] H.J.C. Berendsen, D. van der Spoel, R. van Drunen, GROMACS: A message-passing parallel molecular dynamics implementation, Comput. Phys. Commun. 91 (1995) 43–56, https://doi.org/10.1016/0010-4655(95)00042-E.
[38] D. Van Der Spoel, E. Lindahl, B. Hess, G. Groenhof, A.E. Mark, H.J.C. Berendsen, GROMACS: Fast, flexible, and free, J. Comput. Chem. 26 (2005) 1701–1718, https://doi.org/10.1002/jcc.20291.
[39] A.W. Schüttelkopf, D.M.F. Van Aalten, PRODRG: A tool for high-throughput crystallography of protein-ligand complexes, Acta Crystallogr. Sect. D Biol. Crystallogr. 60 (2004) 1355–1363, https://doi.org/10.1107/S0907444904011679.
[40] T.J. Dolinsky, J.E. Nielsen, J.A. McCammon, N.A. Baker, PDB2PQR: An automated pipeline for the setup of Poisson-Boltzmann electrostatics calculations, Nucleic Acids Res. 32 (2004) W665–W667, https://doi.org/10.1093/nar/gkh381.
[41] P.E. Smith, W.F. van Gunsteren, The viscosity of SPC and SPC/E water at 277 and 300 K, Chem. Phys. Lett. 215 (1993) 315–318, https://doi.org/10.1016/0009-2614(93)85720-9.
[42] S. Miyamoto, P.A. Kollman, Settle: An analytical version of the SHAKE and RATTLE algorithm for rigid water models, J. Comput. Chem. 13 (1992) 952–962, https://doi.org/10.1002/jcc.540130805.
[43] B. Hess, H. Bekker, H.J.C. Berendsen, J.G.E.M. Fraaije, LINCS: A Linear Constraint Solver for molecular simulations, J. Comput. Chem. 18 (1997) 1463–1472, https://doi.org/10.1002/(SICI)1096-987X(199709)18:12<1463::AID-JCC4>3.0.CO;2-H.
[44] T. Darden, D. York, L. Pedersen, Particle mesh Ewald: An N·log(N) method for Ewald sums in large systems, J. Chem. Phys. 98 (1993) 10089–10092, https://doi.org/10.1063/1.464397.
[45] R.W. Hockney, S.P. Goel, J.W. Eastwood, Quiet high-resolution computer models of a plasma, J. Comput. Phys. 14 (1974) 148–158, https://doi.org/10.1016/0021-9991(74)90010-2.
[46] W. Humphrey, A. Dalke, K. Schulten, VMD: Visual molecular dynamics, J. Mol. Graph. 14 (1996) 33–38, https://doi.org/10.1016/0263-7855(96)00018-5.
[47] X. Ying, X. Zhu, D. Li, X. Li, Preparation and specific recognition of protein macromolecularly imprinted polyampholyte hydrogel, Talanta. 192 (2019) 14–23, https://doi.org/10.1016/j.talanta.2018.08.084.